Low-coherence Michelson interferometric fiber-optic multiplexed strain sensor array: a minimum configuration

Libo Yuan, Jun Yang, Limin Zhou, Wei Jin, and Xiaoli Ding

A minimum configuration Michelson fiber-optic low-coherence interferometric quasi-distributed sensing system is proposed that permits absolute length measurement in remote reflective sensor arrays. The sensor's reflective signal characteristics have been analyzed, and the relationship between intensities of light and number of sensors is given for evaluation of multiplexing potential. The proposed sensing scheme will be useful for the measurement of strain distribution. An important application may be strain monitoring in smart structures. Experimentally, four-sensor array has been demonstrated.

OCIS codes: 060.2370, 040.1240, 120.3180.

1. Introduction

Optical sensing systems based on low-coherence interferometry have been intensively investigated in recent years.[1–9] An advantage of this approach compared with using conventional interferometric sensors is well known, in that it can be used to determine a quasi-static measurement such as temperature, pressure, and strain with a corresponding displacement range much larger than one wavelength. Another advantage is that many sensors can be coherently multiplexed onto a single optical signal without the need for relatively complex time or frequency multiplexing techniques. These coherently multiplexed schemes typically use separate receiving interferometers whose time delays are matched to the remote-sensing interferometers.[2] The sensing interferometers are totally passive, and demultiplexed interference signals are insensitive to any changes in length in the connecting fiber leads.

We have designed and demonstrated a minimum configuration Michelson low-coherence interferometric multiplexing sensor array that measures elongation of the absolute optical path lengths between reflectors of each fiber segment. The new approach differs from previously demonstrated multiplexing schemes[2–9] in that only a cavity-length adjustable fiber-optic ring resonator is needed to generate differential optical paths to match the sensing gauges. In the sensor array, only a single fiber lead supplies both input and output signals, which is advantageous because it greatly reduces the complexity and cost of a low-coherence interferometric multiplexed sensor array.

2. Minimum Configuration Low-Coherence Fiber-Optic Michelson Interferometer

The minimum configuration low-coherence fiber optic Michelson interferometer is illustrated in Fig. 1. In this sensing system, only one 2×2 single-mode fiber coupler is used; a LED/P–I–N bidirectional device is used as the light source and as the optical signal detector, thus greatly reducing the size of the interferometer. We couple the broadband LED source of the bidirectional device directly into the fiber sensor array by passing the 3-dB coupler and the fiber ring delay line, in which the delay length is adjustable by a moving prism as shown in Fig. 1. The sensor array consist of N fiber segments (N sensors) connected in series with partial reflectors between adjacent sensors. The reflected signals then travel again in the same path returning to the P–I–N detector of the bidirectional device.

L. Yuan (lbyuan@vip.sina.com) and J. Yang are with the Department of Physics, Harbin Engineering University, Harbin 150001, China. L. Zhou, W. Jin, and X. Ding are with the Hong Kong Polytechnic University, Hong Kong, China; L. Zhou is with the Department of Mechanical Engineering, W. Jin is with the Department of Electrical Engineering, and X. Ding is with the Department of Land Surveying and Geo-Informatics.

Received 13 July 2003; revised manuscript received 24 February 2004; accepted 12 March 2004.

0003-6935/04/163211-06$15.00/0

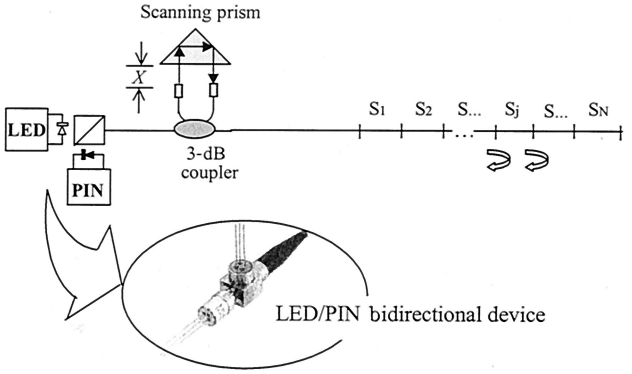

Fig. 1. Minimum configuration Michelson fiber-optic low-coherence interferometric quasi-distributed sensing system.

In the sensing array the reflectivities of the sensors of the in-line reflectors are small (1% or less) to prevent depletion of the input optical signal. The lengths l_j ($j = 1, 2, \ldots, N$) of the fiber sensors between adjacent reflectors have been chosen a little bit longer than but nearly equal to the fixed part of delay length L_0 (or half of resonator cavity length L_0). Each sensor was chosen to be slightly different one the others. The total optical path of the adjustable ring delay line is $nL_0 + 2X$, where X is the distance between the twin gradient-index (GRIN) lens's end surface and the scanning prism. The total optical path of the ring delay line can be tuned through use of a scanning prism–GRIN lens system. When the prism is tuned to a position where the total optical path of the ring delay line is matched to the gauge length of a particular sensor, a low-coherence interferometric pattern is generated.

Take sensor j as an example; the matching paths are shown in Fig. 2(a). The path shown at the top corresponds to the interrogation of sensor j via the right-hand reflective end's surface, whereas the path shown beneath the fiber is for the interrogation via a ring delay line and is reflected by the left-hand end surface of sensor j. Matching of the optical paths is achieved at the same time when

$$nL_0 + 2X_j = nl_j, \qquad j = 1, 2, \ldots, N, \qquad (1)$$

where nL_0 is the path of the ring delay line without including the gap between the prism and the GRIN lenses and can be kept constant by confinement of the system within a heat-isolated box. $X = X_j$ is the distance of the gap between the prism and the GRIN lenses shown in Fig. 1.

The applied strain will cause a change in nl_j that requires a change in gap distance X_j to satisfy the condition given in Eq. (1). The variation in the gap distance (ΔX_j) is related to a change in gauge length by

$$\Delta X_j = \Delta(nl_j)/2, \qquad j = 1, 2, \ldots, N. \qquad (2)$$

For the sensor array we assume that l_1 changes to $l_1 + \Delta l_1$, l_2 changes to $l_2 + \Delta l_2, \cdots$, and l_N changes to $l_N + \Delta l_N$, as distributed stresses are applied to the sensing gauges. Then the distributed strains can be expressed as

$$\varepsilon_1 = \frac{\Delta l_1}{l_1}, \qquad \varepsilon_2 = \frac{\Delta l_2}{l_2}, \ldots, \qquad \varepsilon_N = \frac{\Delta l_N}{l_N}. \qquad (3)$$

To measure the distribution strain, a step-motor positioning system has been used to fine-tune the path length of the scanning prism to match and trace

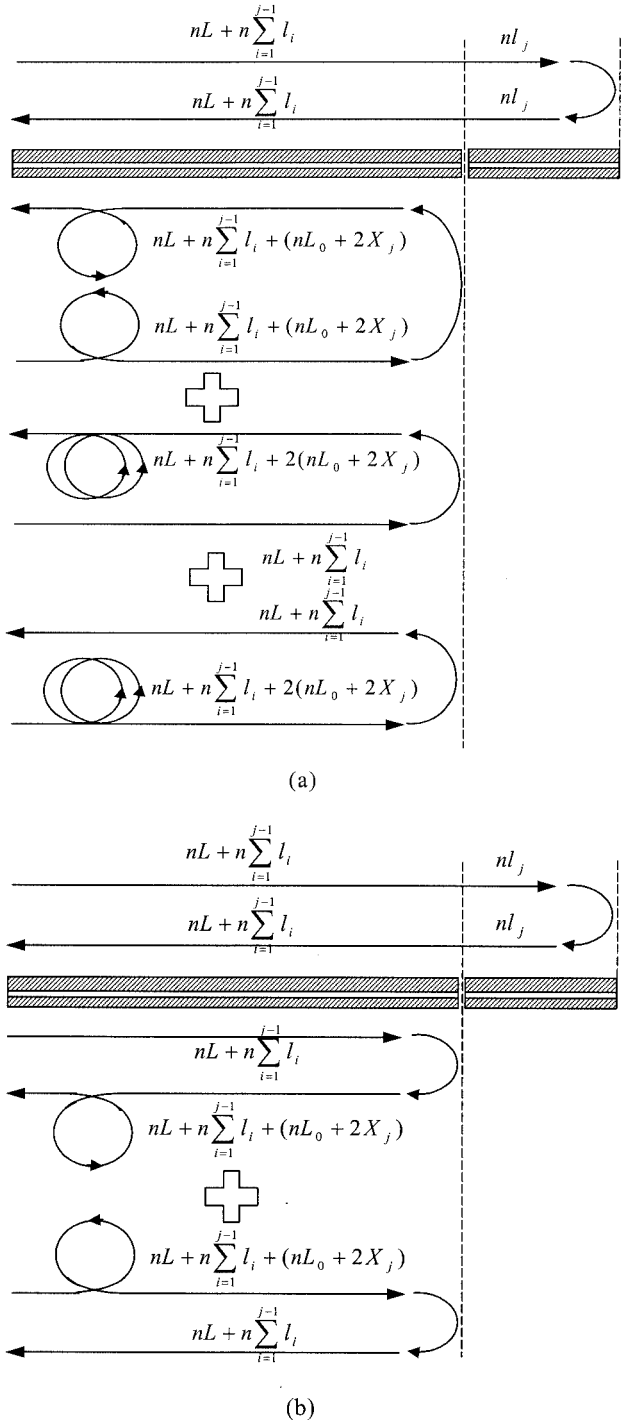

Fig. 2. Equivalent optical paths for sensor j: (a) case 1, $L_0 \approx l_{\text{Sensor}}$; (b) case 2, $L_0 \approx 2l_{\text{Sensor}}$.

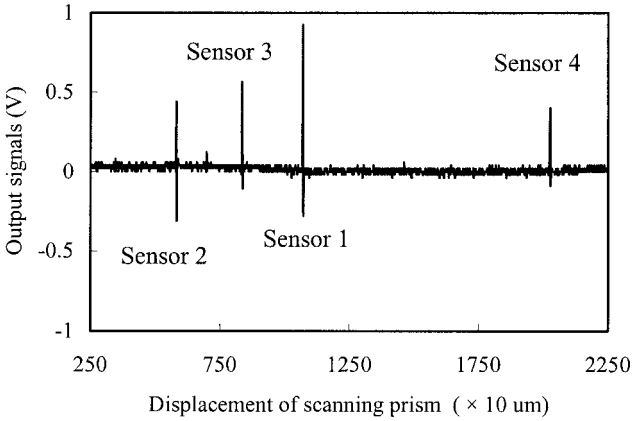

Fig. 3. Experimental scanning peak signals of the four-fiber-optic sensor array.

the variations in lengths of the sensor gauges by Eq. (2). Because each sensor has a unique position, the distributions of strain can be measured by use of Eq. (3).

3. Experimental Results

A four-sensor array was demonstrated in our experiments. In the sensing system the LED's light source power is 30 μW, with a drive current of 50 mA. The insertion losses of a prism–GRIN lens combination is in the range 4–8 dB as the gap distance changes from 3 to 70 mm (corresponding to an optical path change within the range 6–140 mm). The optical path of ring delay line L_0 is chosen as 480 mm, nearly twice the length of the fiber-optic sensor gauge. Each sensor's gauge length is ~250 mm. A 2.2-km-long lead fiber was used in the experiment to permit us to investigate the applicability of this technique for remote sensing. The system output for a value of X that varied from 12.5 to 25 mm is shown in Fig. 3. The four major peaks correspond to the total optical paths of the ring delay line cavities that are matched to the four sensors. From Fig. 3 it is obvious that the gauge lengths of the sensors satisfy $l_4 > l_1 > l_3 > l_2$.

Resolution and accuracy of the system are affected by the relationship of ring delay length and sensor gauge. For fiber-optic sensor j, as shown in the equivalent optical path in Fig. 2(b), if we choose the delay length of the ring to satisfy $L_0 \approx 2l_{\text{Sensor}}$ and adjust X_j over a small range, then the path $(2nL + 2n\sum_{i=1}^{j-1} l_i + 2nl_j)$ can match the path $[2nL + 2n\sum_{i=1}^{j-1} l_i + (nL_0 + 2X_j)]$ and $[(nL_0 + 2X_j) + 2nL + 2n\sum_{i=1}^{j-1} l_i]$, where unwanted interference signals associated with nonadjacent reflectors and nonmatched reflectors lie outside the scan range and are not detected. For this circumstance, we have

$$nL_0 + 2X_j = 2nl_j, \quad j = 1, 2, \ldots, N. \tag{4}$$

In this case the relationship between the changed values in the gap distance (ΔX_j) and the variations of the sensor gauge lengths is given as

$$\Delta X_j = \Delta(nl_j), \qquad j = 1, 2, \ldots, N. \tag{5}$$

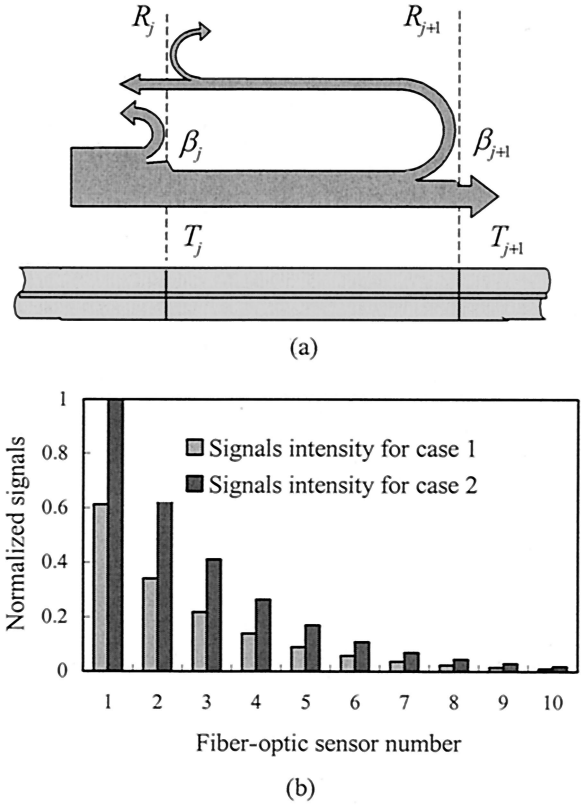

Fig. 4. Results of theoretical simulation: Normalized intensities of optical signals versus number of fiber-optic sensors for case 1, $L_0 \approx l_{\text{Sensor}}$, and case 2, $L_0 \approx 2l_{\text{Sensor}}$. (a) Illustration of the flow of reflective (R) and transmissive (T) signals in fiber-optic sensor j. (b) Intensities of normalized optical signals versus number of fiber-optic sensors.

Compare Eq. (2) with Eq. (5): For the same sensor gauge length, the system's resolution in case 2, described by Eq. (5), is better than in case 1, described by Eq. (2).

In addition, the signals' intensity is gradually decreased as the sensor array size increased, as shown in Fig. 4(a). It is also different in case 1 from that in case 2. The signal intensity from sensor j that is due to coherent mixing between the reflected signals from the two partial reflectors that define the sensor may be expressed as follows:[10]

For case 1

$$P_{D1}(j) = \frac{\sqrt{3}}{2} P_0 \eta(X_j)(R_j R_{j+1})^{1/2} T_j \beta_j \left[\prod_{i=1}^{j-1} (T_i \beta_i)\right]^2; \tag{6}$$

For case 2

$$P_{D2}(j) = \frac{1}{2} P_0 [2\eta(X_j)]^{1/2} (R_j R_{j+1}) T_j \beta_j \left[\prod_{i=1}^{j-1} (T_i \beta_i)\right]^2, \tag{7}$$

where $P_{D1}(j)$ and $P_{D2}(j)$ represent the reflected light intensities from sensor j. P_0 is the light intensity from the LED source coupled into the optical fiber.

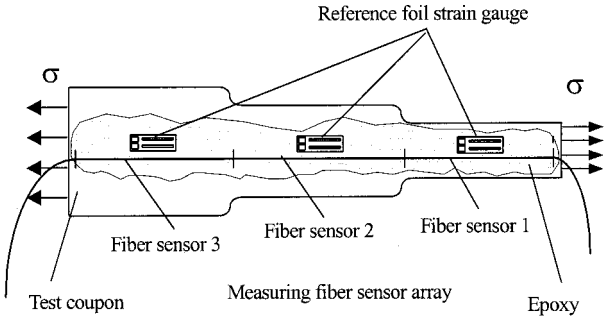

Fig. 5. Experimental setup for test of the fiber-optic strain-sensor array.

The 2×2 couplers are assumed to be 3-dB couplers, and the insertion losses are neglected. β_j represents the excess loss associated with sensor j that is due to a connection loss between the sensing segments. T_j and R_j are, respectively, the transmission and reflection coefficients of the jth partial reflector, as shown in Fig. 4(a). T_j is in general smaller than $1 - R_j$ because of loss factor β_j. $\eta(X_j)$ is the loss associated with the prism's GRIN lens systems and is a function of X_j.

Theoretical simulations were conducted for typical parameters: $\beta_j = 0.9$ $(j = 1, 2, \ldots, N + 1)$, $R_j = 1\%$, $T_j = 0.89$. The average attenuation of the moving prism–GRIN lens combination is taken as 6 dB, i.e., $\eta(X_j) = 1/4$. The power coupled into the input fiber is P_0. The normalized signal intensity for each sensor in the 10 sensors array is shown in Fig. 4(b).

To test the performance of the strain sensor array we made our experiments with a four-sensor array. Each fiber gauge length was nearly equal to 250 mm. Fiber sensors 1–3 were attached to the test specimen, but the fourth fiber sensor was left in a strain-free state. Foil gauges located near fiber sensors 1–3 were used to measure the strains individually. The shape of the test specimen is depicted in Fig. 5. The load was supplied from a load cell to the test specimen and introduced a uniform stress field, σ. Then the corresponding strain was transferred from the test specimen to the optical fiber. As the strain increased, the resultant shift of the interferogram peaks from the fiber-optic interferometer was measured. The testing results from the fiber sensors and the foil gauges are plotted in Fig. 6. It is shown that the fiber-optic sensors could map the applied strain conditions, whereas the fourth, strain-free, sensor was not perturbed, and the sensors' interference pattern peak positions show almost no shift. In addition, the strain or deformation experienced by an optical fiber may not be the same as that of the test specimen, depending on the bonding characteristics between the test specimen and the optical fiber. If the fiber–test specimen bond were perfect, the strain that the fiber-optic sensor experienced would be equal to the strain in the test specimen. However, in practice the fiber has a protective coating made from polymer; therefore, even with a perfect bond, the layered cross section is expected to affect the performance of the fiber-optic sensor. It is obvious that the strain experienced by the optical fiber should

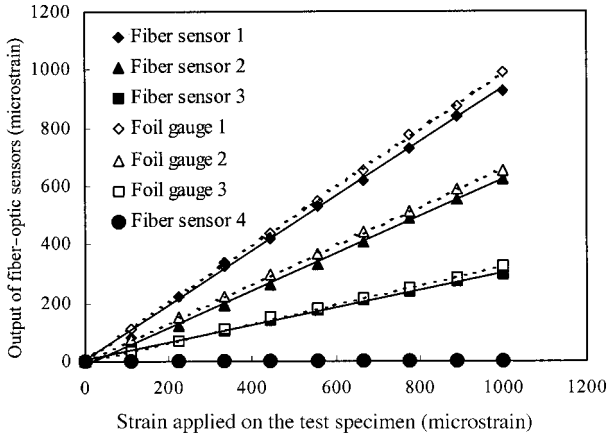

Fig. 6. Performance of the array of fiber-optic strain sensors compared with that of the foil gauges.

always be less than the strain within the test coupon. The test specimen's deformation can be related to fiber's deformation by

$$\varepsilon_{\text{Test}} = \varepsilon_{\text{fiber}}/k. \tag{8}$$

Here k is a constant that depends on the characteristics of the bond between the fiber and the test specimen. Calibrations generally determine the values of k for various bonding conditions. In our case, the average k for the three fiber sensors was measured to be 0.92. The resolution of the strain-sensing system was 5 $\mu\varepsilon$ for the current 250-mm fiber gauge length, and the measuring accuracy was 10 $\mu\varepsilon$.

4. Effects of Polarization

Without special precautions, most interferometric sensors are negatively affected by birefringence and by its effect on the state of polarization of the light propagating in the fiber. This problem is usually addressed by the use of polarization-maintaining fiber.[1] However, using this type of fiber adds a significant cost to a fiber sensing system. It is therefore important to know what the effect of birefringence is on the performance of a particular sensor. In this section we presents an analysis of polarization effects in a low-coherence fiber-optic Michelson interferometric quasi-distributed strain sensor array by considering the effects of a localized region of birefringence-induced polarization states on the sensing fiber's gauge length. For simplicity and clarity we have assumed that the light-wave vector that arrived in the two reflective fiber end faces in sensor j can be expressed as[12]

$$|E_j\rangle = E_0 \exp[-i(\omega t + \phi_j)](\cos\theta_j|P_x\rangle + \sin\theta_j|P_y\rangle), \quad j = 1, 2, \ldots, N + 1, \tag{9}$$

$$|E_{j+1}\rangle = E_{0j+1} \exp[-i(\omega t + \phi_{j+1})](\cos\theta_{j+1}|P_x\rangle + \sin\theta_{j+1}|P_y\rangle), \quad j = 2, \ldots, N, \tag{10}$$

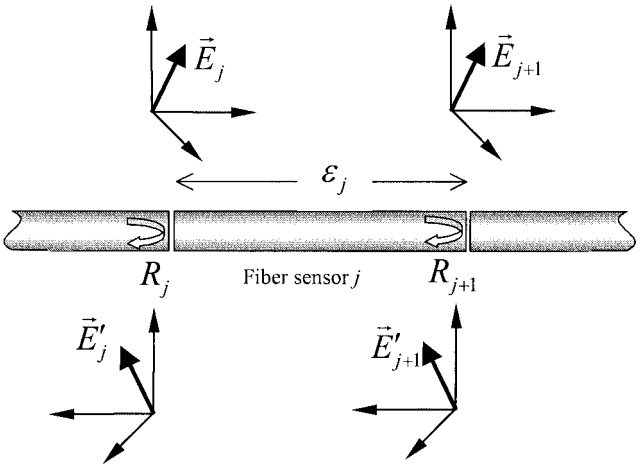

Fig. 7. Strain-induced variation of polarization states between the two reflective fiber ends.

which represent the linearly polarized light-wave vectors in directions θ_j and θ_{j+1} of the jth fiber sensor's two ends. Here ω is the circularity frequency and ϕ_j and ϕ_{j+1} are the phases of the two light waves, E_j and E_{j+1} are the amplitudes of the two light waves, and

$$|P_x\rangle = \begin{pmatrix} 1 \\ 0 \end{pmatrix}, \qquad |P_y\rangle = \begin{pmatrix} 0 \\ 1 \end{pmatrix} \tag{11}$$

are base vectors that represent waves that are linearly polarized in the x and y directions, respectively, as shown in Fig. 7.

Then the reflective light-wave vectors can be expressed as

$$|E_j'\rangle = R_j E_{0j} \exp[-i(\omega t + \phi_j - \pi)][\cos(-\theta_j)|P_x\rangle + \sin(-\theta_j)|P_y\rangle], \quad j = 1, 2, \ldots, N+1, \tag{12}$$

$$|E_{j+1}'\rangle = R_{j+1} E_{0j+1} \exp[-i(\omega t + \phi_{j+1} - \pi)] \times [\cos(-\theta_{j+1})|P_x\rangle + \sin(-\theta_{j+1})|P_y\rangle], \quad j = 2, \ldots, N, \tag{13}$$

where R_j and R_{j+1} represent the reflectivities of the fiber sensor's two ends. Thus the mixing term's output signal intensity can be calculated as

$$\begin{aligned} I_j &= 2\langle E_j'|E_{j+1}'\rangle \\ &= 2R_jR_{j+1}E_{0j}E_{0j+1} \exp\left\{-i\left[(\varphi_{j+1} - \varphi_j) + \frac{4\pi n_c l_j}{\lambda}\right]\right\} \\ &\quad \times (\cos\theta_j\langle P_x| - \sin\theta_j\langle P_y|)(\cos\theta_{j+1}|P_x\rangle \\ &\quad - \sin\theta_{j+1}|P_y\rangle) \\ &= 2R_jR_{j+1}E_{0j}E_{0j+1} \exp\left\{-i\left[(\varphi_{j+1} - \varphi_j) + \frac{4\pi n_c l_j}{\lambda}\right]\right\} \\ &\quad \times (\cos\theta_j\cos\theta_{j+1} + \sin\theta_j\sin\theta_{j+1}) \\ &= 2R_jR_{j+1}E_{0j}E_{0j+1} \exp\left\{-i\left[(\varphi_{j+1} - \varphi_j) + \frac{4\pi n_c l_j}{\lambda}\right]\right\} \\ &\quad \times [\cos(\theta_{j+1} - \theta_j)], \end{aligned} \tag{14}$$

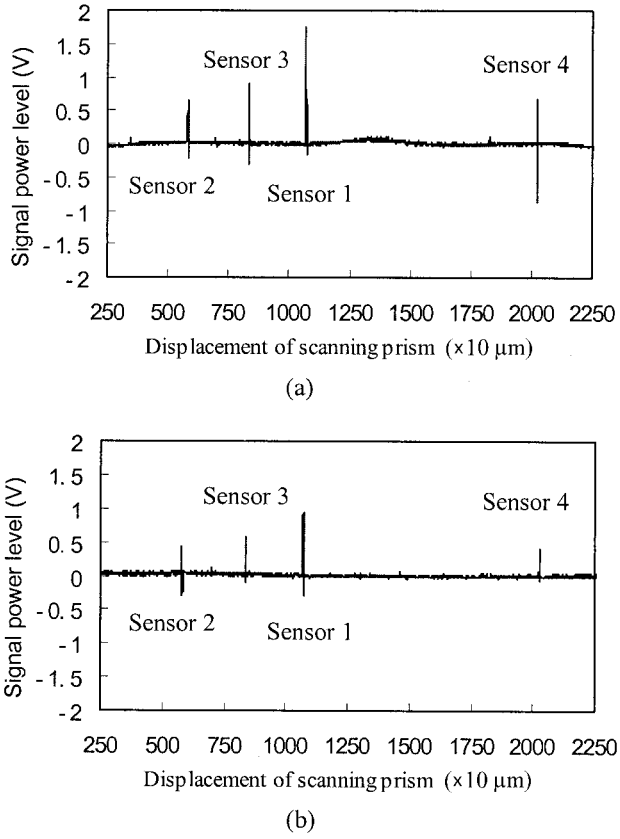

Fig. 8. Effects of polarization states on the array of fiber-optic sensors: (a) amplitudes of the output of a four-fiber sensor array in a strain-free state and (b) change in amplitude of the array after application of 1000 microstrains.

where n_c is the refractive index of the fiber mode, l_j represents the fiber sensor gauge length, and

$$\langle P_x|P_x\rangle = \langle P_y|P_y\rangle = 1, \qquad \langle P_x|P_y\rangle = \langle P_y|P_x\rangle = 0. \tag{15}$$

From Eq. (14) it can be seen that the amplitude of the interferogram peak is related to the difference $(\theta_{j+1} - \theta_j)$ in the directions of the jth fiber sensor two light-wave polarizations. The amplitude of the interferogram peak will fade owing to the localized regional strain-induced birefringence in each fiber sensor (fiber segment). The experimental results of polarization fading are shown in Fig. 8. The amplitude of the output signal of each fiber sensor faded when 1000 microstrains were applied to the four-sensor array. Normally one would expect that birefringence would be randomly distributed in a fiber sensor array. Therefore it is difficult to control the polarization states in a fiber-optic sensor. However, in a white-light fiber-optic interferometric sensing system the tolerance is big enough because the measurement result just depends on the interferogram's peak position, and it is independent of the amplitude of the interferogram's peak.

5. Conclusions

In conclusion, based on a LED/P–I–N bidirectional device, a multiplexed fiber-optic deformation sensor array suitable for smart structure applications has been designed and demonstrated. The sensor array systems are based on a white-light Michelson interferometric technique. The sensor array is completely passive, and an absolute length measurement can be obtained for each sensing fiber segment so it can be used to measure quasi-distribution strain or temperature. For large-scale smart structures this technique not only extends the multiplexing potential but also provides a reduced optical structure and low-cost sensing system. Polarization fading can cause some problems, but it can be minimized by introduction of polarization-maintaining fiber during fabrication of the fiber sensor array.

This research was supported by the National Nature Science Foundation of China under grant 50179007 and by a grant from The Teaching and Research Award Program for Outstanding Young Professors in Higher Education Institute Ministry of Education, China, to Harbin Engineering University.

References

1. G. Beheim, "Remote displacement measurement using a passive interferometer with a fiber-optic link," Appl. Opt. **24,** 2335–2340 (1985).
2. J. L. Brooks, R. H. Wentworth, R. C. Youngquist, M. Tur, B. Y. Kim, and H. J. Shaw, "Coherence multiplexing of fiber optic interferometric sensors," J. Lightwave Technol. **LT-3,** 1062–1071 (1985).
3. H. C. Lefevre, "White light interferometry in optical fiber sensors," *Proceedings of the Seventh Optical Fiber Sensors Conference* (Information, Telecommunications & Electronics Engineering Society, Sydney, Australia, 1990), pp. 345–351.
4. C. E. Lee and H. F. Taylor, "Fiber-optic Fabry–Perot temperature sensor using a low-coherence light source," J. Lightwave Technol. **9,** 129–134 (1991).
5. A. B. L. Ribeiro and D. A. Jackson, "Low coherence fiber optic system for remote sensors illuminated by a 1.3-μm multimode laser diode," Rev. Sci. Instrum. **64,** 2974–2977 (1993).
6. D. Inaudi, A. Elamari, L. Pflug, N. Gisin, J. Breguet, and S. Vurpillot, "Low-coherence deformation sensors for the monitoring of civil-engineering structures," Sensors Actuators A **44,** 125–130 (1994).
7. W. V. Sorin and D. M. Baney, "Multiplexing sensing using optical low-coherence reflectometry," IEEE Photon. Technol. Lett. **7,** 917–919 (1995).
8. L. B. Yuan and F. Ansari, "White light interferometric fiber-optic distributed strain-sensing system," Sensors Actuators A **63,** 177–181 (1997).
9. L. B. Yuan, L. M. Zhou, and W. Jin, "Quasi-distributed strain sensing with white-light interferometry: a novel approach," Opt. Lett. **25,** 1074–1076 (2000).
10. L. Yuan, L. Zhou, W. Jin, and J. Yang, "Design of a fiber-optic quasi-distributed strain sensors ring network based on a white-light interferometric multiplexing technique," Appl. Opt. **41,** 7205–7211 (2002).
11. A. A. Chtcherbakov and P. L. Swart, "Polarization effects in the Sagnac–Michelson distributed disturbance location sensor," J. Lightwave Technol. **16,** 1404–1412 (1998).
12. L.-B. Yuan and L.-M. Zhou, "Fiber optic moiré interference principle," Opt. Fiber Technol. **4,** 224–232 (1998).